Dynamics of phototunable two-dimensional polar wetting sheets of a dendritic liquid crystal

Satoshi Aya,[1,*] Takaaki Hikima,[2] Osamu Haba,[3] Koichiro Yonetake,[3] and Fumito Araoka[1,†]
[1]*RIKEN Center for Emergent Matter Science (CEMS), 2-1 Hirosawa, Wako, Saitama 351-0198, Japan*
[2]*RIKEN SPring-8 Center, 1-1-1 Kouto, Sayo, Hyogo 679-5148, Japan*
[3]*Graduate School of Organic Materials Science, Yamagata University, 4-3-6 Jonan, Yonezawa, Yamagata 992-8510, Japan*

(Received 18 September 2018; published 2 November 2018)

Azobenzene-based molecular systems are used as photoreswitchable smart materials with applications in many areas, including designing surface orientational patterning of anisotropic molecules. It is important and challenging to probe the real-time photoresponsive behaviors of these systems, particularly the photodynamic processes from the mesoscopic to microscopic or macroscopic scales near surfaces. We report an unusual reversible interfacial wetting-dewetting switching of a dendrimer incorporating azobenzene moieties. The switching is accompanied by light-driven generation or extinction processes of the surface wetting nanostructures, which are composed of supramolecular polarly layered molecules. The resultant polar-nonpolar switching of the surface allows macroscopic wetting-dewetting and nonlinear optical responses. Our results provide unique insights into controlling transient structures of photoresponsive materials.

DOI: 10.1103/PhysRevE.98.052701

I. INTRODUCTION

Azobenzene-based materials have received considerable attention because their dynamic photoresponsivity allows efficient reversible physicochemical property conversion (e.g., polarity variation) arising from *cis-trans* isomerization. In particular, azobenzene-based materials are used as photoresponsive command surfaces for aligning anisotropic molecules [1]. Azobenzene-based command surfaces offer precise control over the orientation of molecules with (sub-) micrometer spatial resolution. Thus, azobenzene-based materials are essential in liquid crystal (LC) displays [2] and optical elements [3,4]. Exploiting the dynamic properties of azobenzene has been a central focus of many applications, such as photosensitive actuators [5] and active molecular tweezers [6,7]. Hence, it is important to clarify the azobenzene molecule superstructures photodynamic properties, which govern the macroscopic changes in physicochemical properties, at different spatial length scales.

Over the past few decades, the dynamic structural variation due to photoresponsivity in azobenzene moleucles has been studied at the molecular scale and at the submicron to micron scale, including mass-transport phenomena. Spectroscopic studies have clarified the behavior of azobenzene molecules at the molecular scale. For instance, *trans*- and *cis*-isomers coexist at a specific molar ratio at equilibrium, in accordance with environmental parameters, such as temperature, light intensity, and the spectral distribution of the irradiated light. The change in the orientation of the molecular end group of the azobenzene molecules mediated by the conformational change around the azobenzene linkage alters the orientation of the anisotropic molecules in contact with the azobenzene-decorated surfaces. The behavior of azobenzene molecules at the submicron to micron scale has been explained theoretically based on the dynamic behavior of azobenzene molecules in terms of the relationship between the microscopic and macroscopic changes, for instance, the Weigert effect [8,9], mean-field theory [10], permittivity gradient theory [11], and the gradient electric force model [12].

In this paper, we explore the photodynamics of the surface-localized nanostructure of a dendrimer incorporating azobenzene units [AzD6; see the structure in Fig. 1(a)], suspended in a host anisotropic fluid of a nematic molecule, 4-cyano-4′-pentylbiphenyl (5CB). This type of dendrimer tends to self-segregate and decorate the substrate surface to give specific anchoring conditions for nematic liquid crystals (NLC) [13]. Therefore, the AzD6-decorated surface provides a unique platform for photodynamic wetting via *cis-trans* isomerization upon light stimulation. So far, the surface photoresponsivity of the AzD6-doped NLC was reported in different geometries [14–16], and a surface monolayer AzD6 was assumed to change the anchoring conditions. However, it is yet unclear as to how the AzD6 molecules are arranged on surfaces.

Because the surface-localized nanostructure exhibits a nanometer-thick lamellar structure similar to that in Ref. [17] and can reversibly wet or dewet surfaces in response to light, we refer to these structures to as surface wetting sheets (SWS). The dynamic processes in the AzD6 SWS upon light irradiation or thermal relaxation are clarified by the real time observation methods grazing-incidence x-ray diffraction (GIXRD) and transient second-harmonic generation (SHG). Based on these analyses, we discuss the dynamics of extinction and generation or growth processes of the AzD6 SWS, which is found to carry polar ordering. In addition, in the light of the relationship between SWS structure and the orientation of host NLC molecules, we show that the self-segregated photoresponsive SWS stabilizes the homeotropic (H) alignment state of the NLC and the alignment state of the NLC

*satoshi.aya@riken.jp
†fumito.araoka@riken.jp

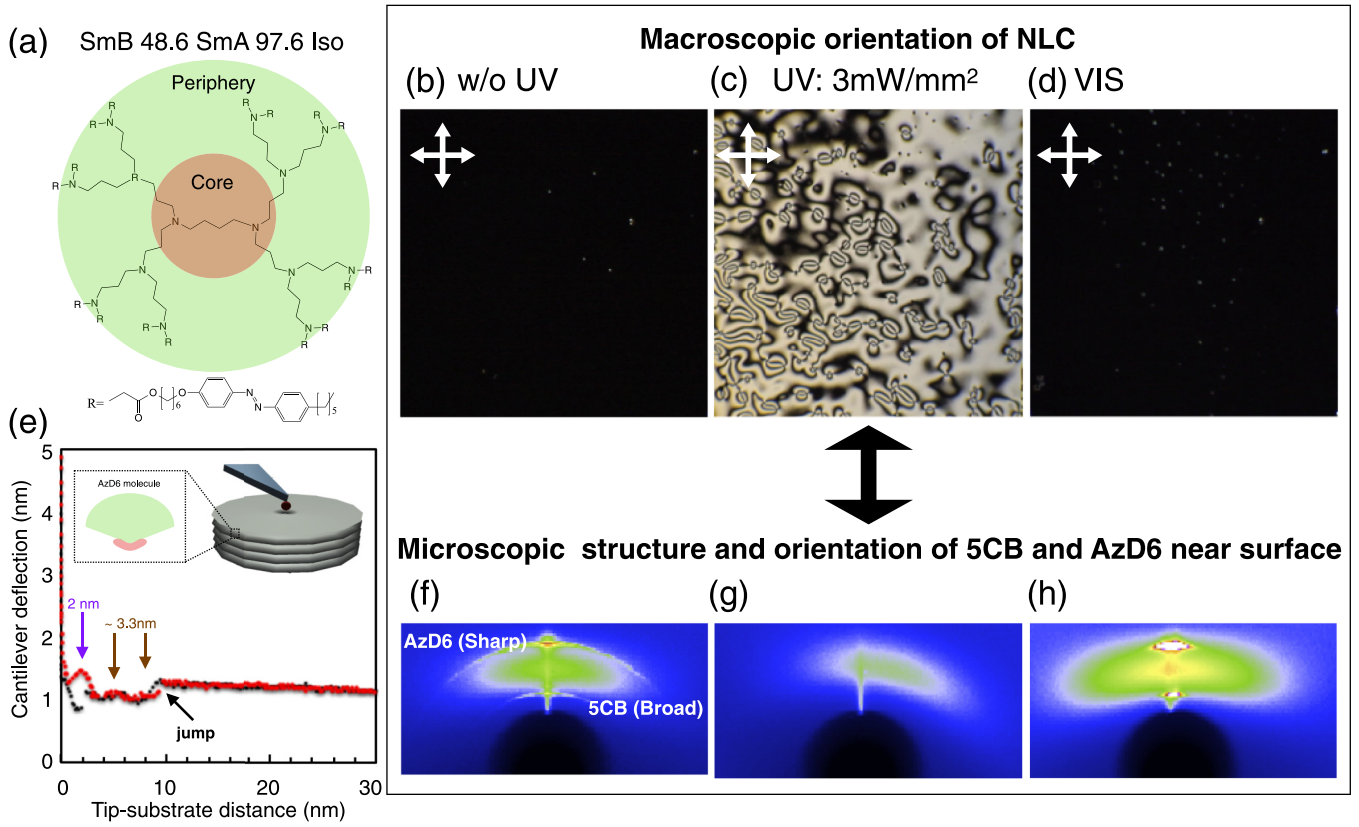

FIG. 1. (a) Molecular structure of AzD6 and its phase sequence. (b)–(d) Texture variation of 1 wt% AzD6/5CB mixture in an LC cell (b) before and (c) after 3 mW/mm^2 UV irradiation, and (d) after Vis irradiation. Scale bar is 100 μm. (e) Force curve measurement of AzD6 film left from 1 wt% AzD6/5CB mixture after washing 5CB away with isopropanol. (f)–(h) Corresponding variation of v-GIXRD diffraction patterns for the conditions in (b)–(d).

can be tuned by light stimuli because of the extinction and regeneration of the SWS near the surface.

II. EXPERIMENTAL

A. Materials

Neat AzD6 exhibits mesophases as given in the phase sequence: smectic B – 48.6°C–smectic A – 97.6°C–isotropic liquid (I). The 5CB NLC has the phase sequence crystal – 22°C – N – 35.4°C–I. For observations of AzD6 itself, unless otherwise stated, a spin-coated film was fabricated on a glass substrate from a chloroform solution. The equilibrium state of the film was ensured by annealing the film in the I phase for 30 min. For observations of the AzD6-doped NLC, 0.1 wt% AzD6 was added to 5CB prior to injecting it into an LC cell.

B. Force curve measurements

To probe the microscopic elastic behavior of SWS on a flat surface [18,19], force curve measurements were conducted using a scanning probe microscope (SPM-9700, Shimadzu) by contact mode atomic force microscopy (AFM). AFM images and force curves were obtained concurrently. We used a ϕ10-μm colloidal probe with a force constant of 0.32 N/m (CP-PNPS-BSG-C, NanoWorld) for the measurements. The probe tip was cleaned with detergent and rinsed with milli-Q water. After washing the probe in a propanol solution at 100°C, *N,N*-dimethyl-*N*-octadecyl-3-aminopropyltrimethoxysilyl chloride, which induces H alignment of NLCs, was deposited on the probe based on the procedure described in Ref. [20].

C. Polarizing optical microscopy

Textures were recorded using a commercial polarizing microscope (Eclipse LV100 POL, Nikon) equipped with a digital camera. All the polarizing optical microscopy (POM) images in this study were taken with crossed nicols.

D. GIXRD measurements

All GIXRD measurements (incident angle, 0.05°) were carried out at RIKEN structural biology beamline I (BL45XU) (λ = 1 Å) in SPring-8 [21]. The beam diameter was about 0.3 mm. Measurements were made by accumulating the diffraction signals over 1 s. A neat film of AzD6, or droplets of either AzD6-doped 5CB or AzD6-doped water was prepared on both silicon and glass substrates. To distinguish the bulk and surface signals, measurements were performed by vertically scanning the sample placed flat on a motorized translation stage and recording the signals in steps of 1 μm. In the video-rate GIXRD (v-GIXRD) measurements, the dynamics were traced at a time resolution better than 0.2 s per frame.

E. SHG measurements

Second harmonic (SH) signals were captured using a homemade system. We used a fundamental beam from a Ti:sapphire oscillator (Vitesse 800, Coherent) with a central wavelength of 800 nm, maximum power of 280 mW, pulse duration of 120 fs, and 80 MHz repetition. The p-polarized fundamental beam was directed at either films or LC cells. The SH light was filtered to be p-polarized and detected from the transmission direction by a cooled photomultiplier tube (H7732P-01, Hamamatsu) with a photon counter module (C8855-01, Hamamatsu). The gate time for counting was set to 1 s, and accordingly the recorded data has a time resolution of 1 s.

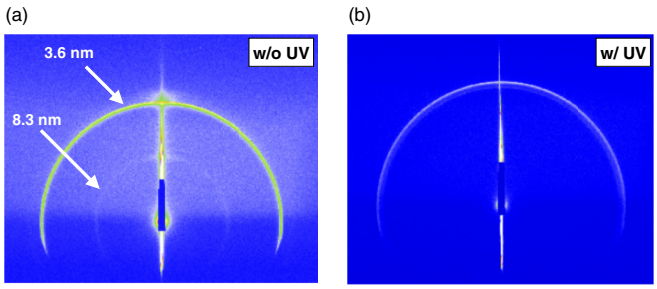

FIG. 2. GIXRD measurement on a spin-coated 100-μm thick AzD6 film. (a) and (b) Small angle GIXRD diffraction patterns of the AzD6 film at conditions of without UV irradiation (a) and upon 3 mW/mm^2 UV irradiation (b).

III. RESULTS AND DISCUSSION

First, we examined a sample in an LC cell made of two glass substrates with no surface modification, and the H state was induced spontaneously (Movie S1) [22] by self-segregation of AzD6 on the surfaces, as previously reported [13,15,16,23]. The H state [Fig. 1(b)] realigns to a planar (P) state [Fig. 1(c)] upon UV exposure with a UV LED lamp (365 nm) exceeding a critical light strength ($I_{\mathrm{UV,C}} = 0.4\,\mathrm{mW/mm^2}$), thereby exhibiting birefringence under POM. This is attributed to the *trans-cis* isomerization through the π-π^* transition of the azobenzene part induced by the UV excitation. Note that the discontinuous nature from the H to P state can be observed only when visible (Vis) light from the illumination lamp of POM is weak enough, in which situation the back induction induced by the POM illumination from *cis*- to *trans*-state can be neglected. After switching off the UV light, the H state was regenerated by either thermal relaxation or Vis exposure at 512 nm from a laser diode [Fig. 1(d)], mediated by the *cis-trans* back-isomerization caused by the n-π^* transition.

GIXRD and force curve measurements were conducted to reveal the microscopic self-assembled structure of AzD6 near the interface between the substrate surface and the bulk of the AzD6-doped NLC. In the GIXRD measurements, a 5-μL droplet of AzD6-doped NLC was placed on a glass substrate, and irradiated with an x-ray beam. For comparison, a bulk AzD6 film of 100 μm at different light illumination conditions was also investigated. Figures 1(f)–1(h) show small-angle diffraction (SAD) patterns in the states corresponding to the texture variation in Figs. 1(b)–1(d), respectively. Without UV exposure, the SAD pattern [Fig. 1(f)] contained a set of sharp peaks at $d = 3.6$ nm and 2.1 nm, and an indistinct peak at $d = 2.5$ nm, which appeared in the direction of the substrate normal. The sharp peak for AzD6 at 2.1 nm has never been observed in the bulk [24], suggesting surface-induced ordering, that is, the AzD6 SWS. Because the d value of 2.1 nm was much shorter than half of the calculated stretched length (7.8 nm) of AzD6 [23,24], the molecules adopt a folded or bowlic conformation with the side mesogenic arms deviating from the surface normal [see the inset schematics of Fig. 1(e)]. Although Li *et al.* observed the same sharp peak at $d = 3.6$ nm and assigned it to the second-order diffraction of the smectic layers of stretched AzD6 [24], GIXRD detected a weak peak locating in the range of 8.3 nm, but no peak around $d \sim$ 7.2 nm which should correspond to the first-order diffraction, in the 100-μm bulk AzD6 film. The 8.3-nm peak disappears when a UV light is illuminated (Fig. 2). However, the d value of 3.6 nm is almost half the molecular length of AzD6. Even if the molecules adopt either the folded or bowlic conformation, the lamellar layer spacing should be shorter than the half of the stretched molecular length, and this was the case for the peak at $d = 2.1$ nm observed near the surface. Thus, we suggest an interdigitated smectic structure of AzD6 as a plausible bulk structure, similar to those observed in some LC systems [25]. The indistinct peak at $d = 2.5$ nm is consistent with the nematic ordering of AzD6-doped NLC in the H state. As the UV intensity I_{UV} was increased, the AzD6 SWS started to melt, and the corresponding peak disappeared at the critical UV intensity $I_{\mathrm{UV,C}}$ of $\sim$0.4 mW/mm^2 [Fig. 1(g)]. This threshold value is consistent with the results reported in Ref. [26]. The existence of the threshold suggests that there is a critical molar balance between *trans*- and *cis*-isomers to trigger the disruption of SWS. Above $I_{\mathrm{UV,C}}$, NLC began to adopt the P state instead of the H state, as indicated by the peak position tilted from the surface normal direction [Fig. 1(g)]. This result confirms that the SWS on the surface was coupled to the orientational order of the NLC and commanded the director normal to the surface. Further discussion of the variation of the longitudinal correlation length ξ, which is proportional to the second-order order parameter, may provide a better understanding of this behavior. Upon UV exposure, ξ of AzD6 decreased continuously in a narrow low-UV-strength window until $I_{\mathrm{UV,C}}$, whereas ξ of NLC did not change in this region [Figs. 3(a) and 3(b)]. Instead, ξ of NLC decreased above $I_{\mathrm{UV,C}}$ after the SWS melted completely. This quantitative result suggests that the SWS had the following major effects on the orientation of NLC: The top surface of the SWS anchored the NLC vertical to the surface and induced the H state as a bulk orientation; the SWS increased the order parameter of the NLC near the surface. Once the SWS diminishes, the H state cannot be maintained by the surface anymore and the order parameter of the NLC near the surface relaxes back to its bulk value. Conversely, Vis exposure coupled the back switching of NLC, from the P to the H state, was also coupled to the regeneration of the SWS [Figs. 1(d) and 1(h)]. Above a critical Vis intensity, $I_{\mathrm{Vis,C}} \sim 14.5\,\mathrm{mW/mm^2}$, the SWS was regenerated, and then ξ of AzD6 increased with increasing Vis intensity I_{Vis}. At the same time, ξ of the NLC increased and

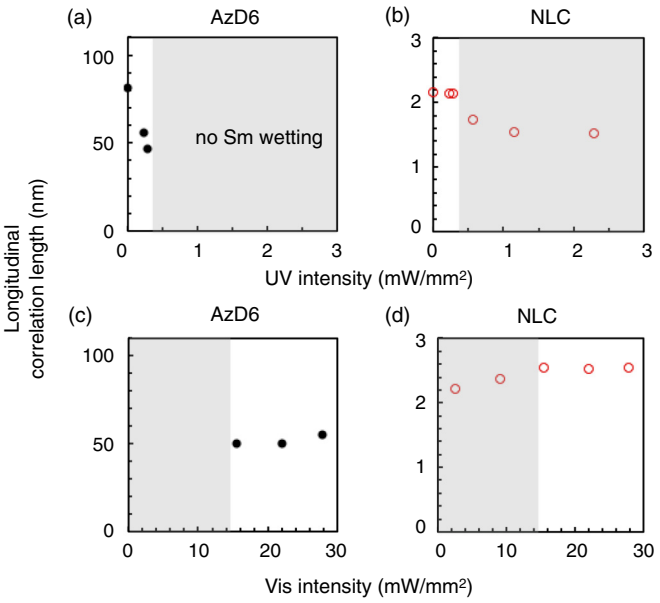

FIG. 3. Variation of longitudinal correlation length of 5CB and AzD6 calculated from the full width at half maxima of the GIXRD SAD, with UV and Vis light strength.

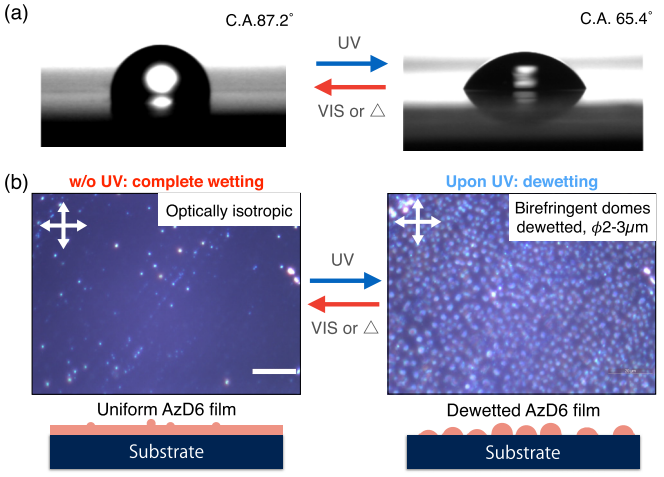

FIG. 4. (a) Contact angle measurement of a water droplet on the corresponding AzD6. The contrast of the pictures was adjusted to improve visibility. (b) Texture variation of a pure AzD6 film on a glass substrate before and upon UV irradiation with schematics. Scale bar is 20 μm.

became saturated as the SWS was regenerated [Figs. 3(c) and 3(d)].

In the force curve measurements, the colloidal probe was pressed onto the AzD6 surface layer that remained after washing AzD6-doped NLC away by isopropyl alcohol. This washing technique was also used in Ref. [13]. Figure 1(e) shows the force curves obtained during the approach (red dots) and retraction (black dots) of the probe. Upon the approach, the cantilever jumped into contact with AzD6 at a distance of ~10 nm. As the probe approached further, the force curve oscillated because of the periodic elastic lamellar layers. The diverging force at zero distance indicated the hard contact between the cantilever and the substrate. This result confirms that, even in the AzD6-doped NLC, the SWS structure was parallel to the surface. Counting the number of oscillations before the hard contact showed that at least two or three lamellar layers wet the surface. The thickness of the nearest-surface layer was about 2 nm and the oscillating periodicity of the subsequent layers far from the substrate was about 3.3 nm. Both are consistent with the GIXRD peaks, which supported our proposed structure. First, the AzD6 molecules were folded or curved into an asymmetric configuration, at least near the surface. The amplitude of the nearest-neighbor peak to the substrate was considerably larger than the others; thus, the first lamellar layer adsorbed onto the surface was more robust owing to the presence of the surface. Second, our force curve experiment did not show periodicity corresponding to the fully stretched molecular length of AzD6 (7.8 nm) or the previously reported d value of d = 6.7 nm [24]. Instead, the periodicity of 3.3 nm was observed in our force curves, which suggest the bulk interdigitated smectic structure formed above SWS. Thus, the force curves indicate the formation of lamellar SWS and the interdigitated smectic structure on top. Even during the probe extraction, a weak oscillatory force was observed. The difference from the probe approach was attributed to the pressure-induced deformation of SWS during the approach. We also measured the force curve during UV light irradiation at 365 nm, which promotes the *trans-cis* isomerization. In this case, force curves could not be obtained due to the substantial reduction of viscoelasticity due to the structural melting of the SWS induced by UV light.

Because the reversible interfacial structural variation controlled by light changes the surface tension, the AzD6 film was expected to serve as a switchable wetting surface. Figure 4(a) shows the contact angle switching of a water droplet placed on an AzD6 film after washing AzD6-doped NLC away by isopropyl alcohol. Before UV exposure, a larger contact angle of 87.2° was observed. Considering the hydrophilic core of AzD6 is contacting with the substrate while hydrophobic arms of AzD6 are stretched outward from the substrate, the large contact angle is attributed to the high hydrophobicity and low surface energy of the AzD6 SWS in the *trans-rich* state. After UV irradiation, the switching of surface wettability was clearly observed by the reshaping of the droplet as the contact angle changed to 65.4°. Thus, a photoresponsive smart surface with switchable wettability was realized.

Li *et al.* reported the dewetting behavior of AzD6 films that formed micro-domes, only when the film thickness is less than 100 nm, from a uniform state by UV irradiation at a power of 5 mW [24]. This geometrical variation can also affect the contact angle. When we prepared a spin-coated film of the neat AzD6 (~1 μm), similar dewetting behavior was also observed by POM at UV intensities larger than ~1 mW/mm^2 [Fig. 4(b)]. The POM texture with UV exposure showed an optically isotropic state, suggesting that homogeneous SWS layers were stacked on the surface. When the sample was subjected to UV stronger than $I_{UV,C}$, this spatial uniformity was disturbed and microdomes appeared. At the same time, birefringence arose in each microdome, as a likely consequence of breaking of the SWS structure, resulting in the dewetting-induced change in the curvature of the SWS. When the film was exposed to Vis, unexpectedly, the

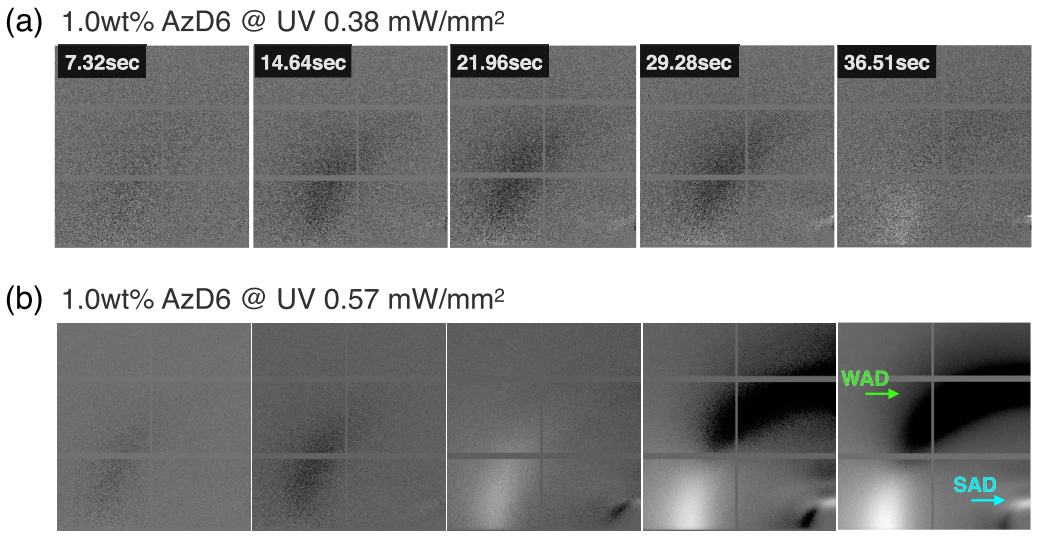

FIG. 5. Snapshots of v-GIXRD upon light irradiation calculated by image subtraction (the computation procedure is given in the main text) at two UV intensities. White regions indicate disappeared signals, and black regions are emerging signals at a given time.

dewetted microdomes continuously transformed back to the initial optically isotropic state. The regenerated dark texture contained some small bright dots, which were not seen before UV exposure. This may be because the back transformation upon Vis exposure was accompanied by the nucleation and growth of the SWS. The observations suggest that the surface wetting can be repeatedly switched by light stimuli in a reversible manner, which is only rarely seen in rigid LC phases [27].

The GIXRD data are time averaged and lack the transient information about structural and orientational variation; thus, we performed v-GIXRD with a capture rate of 5 fps (50 ms on-gate time for x-ray exposure and 150 ms off-gate time for the next exposure). Figure 5 shows v-GIXRD snapshots for 1 wt% AzD6-doped NLC, obtained by the subtraction technique. Transient subtraction images were obtained by subtracting the initial image at which UV exposure started. In these snapshots, SAD (indicated by red arrows) and the indistinct wide-angle diffraction (WAD, indicated by green arrows) signals are shown for the following UV light conditions: (1) at $I_{UV} = 0.38\,mW/mm^2$ ($< I_{UV,C}$); (2) at $I_{UV} = 0.57\,mW/mm^2$ ($> I_{UV,C}$). The WAD spots corresponded to the transverse intermolecular correlation of the NLC. The higher contrast in the patterns indicates a greater change from the initial state. Black and white represent the induction and reduction of the diffraction signals, respectively. For condition (1), there was only a slight change even 37 s after UV irradiation began [Fig. 5(a)]: As the sharp SAD signals of SWS decreased slightly, the WAD pattern became more isotropic. This weak UV irradiation would only melt a tiny portion of the SWS, so the reduction of the SWS surface coverage was small. Therefore, the H state of the host NLC was maintained despite a small reduction in the order parameter. However, for condition (2), both the SAD and the WAD patterns changed significantly with time. At 21.96 s, the SAD signal around the meridian plane and the WAD signal around the equator plane disappeared. Later, a distinctly different pattern evolved [Fig. 5(b)], confirming that the SWS extinction was complete and the H state of the NLC collapsed into a nonaligned state. This sequence confirmed in real time that the extinction of SWS and the reorientation of NLC were intercorrelated.

By considering both the surface energy and the photoinduced kinetic equations of *trans-cis* isomerization, the transitional nature of the light-driven variation in the SWS and its impact on NLC alignment can be understood. On one hand, the modified Rapini-Papoular equation based on the two easy axes model is adapted to the present system similarly to Ref. [17]. This gives a double-well potential curve with its minimum at the H and tilted states, enabling the discontinuous variation in the orientation of the host NLC as a function of light intensity. On the other hand, the surface anchoring energy W_a can also be assumed to be a function of isomerization-relaxation rate and light intensity: $W_a = \kappa(\frac{1}{\eta} - \eta)$, where κ is a scaling factor and $\eta = \frac{k_{tc} I_{UV}}{k_{ct} I_{Vis}}$ is a ratio related to *trans*-to-*cis* and *cis*-to-*trans* relaxation transition coefficients (k_{tc}, k_{ct}), and UV and Vis light intensities (I_{UV} and I_{Vis}) [26]. Since the two models are equivalent, equating the equations of the models discloses that the H state can persist at the most stable state when η is small (I_{UV} is weak) but transits to the tilted state when η exceeds a certain threshold value. This conclusion is consistent with our previous modeling [17,26].

Lastly, we discuss the photodynamic behavior of SWS in an LC cell by SHG, the optical configuration of which is shown in Fig. 6(a). This is a nonlinear optical technique that can detect surface-specific symmetry breaking in real time. The technique complements the v-GIXRD data, providing structural and analytical information on the surface dynamics involving the regeneration process of SWS. Figure 6(b) shows time evolution of an SH signal taken during the regeneration process of SWS prompted by thermal excitation (at 25°C), where the *cis-trans* back-isomerization takes place. This photoswitching can be repeated [Fig. 6(c)]. In this experiment, the pp-polarization combination was used, as described in the Experimental section, and the other polarization combinations showed signals too small to be detected. Thus, the observed SH signals were attributed to the asymmetric polar structure of SWS [see the cartoon in Fig. 6(d)]. This result demonstrates that sufficiently strong UV irradiation decreased the SH sig-

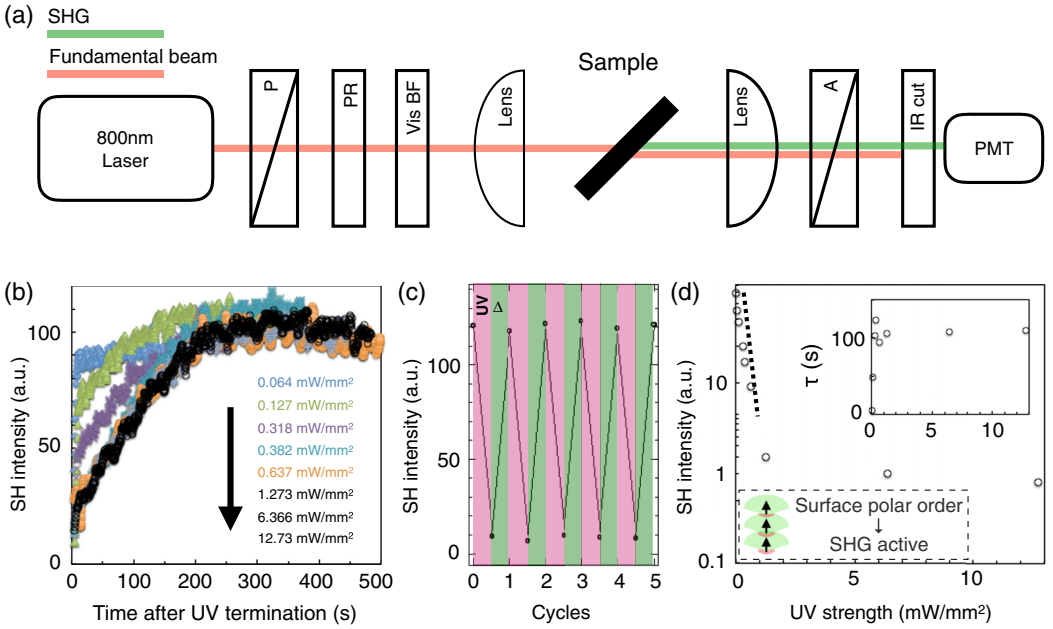

FIG. 6. (a) Schematic of SHG measuring system. The labels P, PR and A mean polarizer, polarization rotator and analyzer, respectively. (b) SH signal as a function of time after UV irradiation at different UV intensities. Time 0 is the time the UV irradiation is stopped. (c) Variation of SH intensity under alternating UV light irradiation (12.73 $\mathrm{mW/mm^2}$) and thermal relaxation. (d) SH signal at time 0 in (b) as a function of UV strength. The inset shows the relaxation time from the signal level at time 0 to the initial level [saturated level in (b)] as a function of UV strength.

nal. After the UV irradiation ended, the signal relaxed slowly back close to the original signal level before UV exposure. These observations suggest that once a larger number of SWS are destroyed by stronger UV exposure, the speed of regeneration of these wetting sheets decreases according to I_{UV}. The SH intensity just after UV exposure (at time 0) was proportional to I_{UV} in the region of $I_{\mathrm{UV}} < 1.5\,\mathrm{mW/mm^2}$ [Fig. 6(d)]. In the region of $I_{\mathrm{UV}} > 1.5\,\mathrm{mW/mm^2}$, the SH signal remained small due to the complete melting of SWS. The inset of Fig. 6(d) shows the I_{UV} dependence of the signal relaxation time τ, which corresponds to the regeneration time of SWS. This result shows that the time required for regeneration was almost inversely proportional to the coverage of the molten SWS, according to $\tau \propto I_{\mathrm{UV}}$. This relationship means the regeneration process is a single process, which is an analog of elementary reactions in chemistry [28].

By analyzing SH signal on the Avrami scale, the kinetics of the SWS regeneration process can be obtained. Figure 7(a) shows an Avrami plot of SH signal under two regimes ($I_{\mathrm{UV}} < I_{\mathrm{UV,C}}$ or $I_{\mathrm{UV}} > I_{\mathrm{UV,C}}$) according to the Avrami equation, $\ln[\ln(1/(1-X))] = n \ln t + \ln K$ [29–32], where X, K, t, and n are the volume fraction of SWS, the temperature-dependent Avrami constant, time, and the Avrami coefficient, respectively. Because the SH signal is considered to originate purely from the SWS, we assumed that X was proportional to the SH intensity. This means that the AzD6 molecules were polarly packed in growing SWS domains, which supports the GIXRD results showing the asymmetric arrangement of AzD6 [the cartoon of Fig. 6(d)]. The fitting results for two Avrami coefficients as a function of I_{UV} are shown in Fig. 7(b). On the one hand, $n = 1$ indicates heterogeneous nucleation with interface-controlled one-dimensional or diffusion-limited two-dimensional growth. Considering that the AzD6 molecules stack in a polar manner, interface-controlled one-dimensional growth is more plausible than diffusion-limited two-dimensional growth. On the other hand, $n = 1/2$ indicates heterogeneous nucleation with diffusion-limited one-dimensional growth [33]. The Avrami analysis for the growth of AzD6 in the SmB phase, for which we measured the SWS by transient optical absorbance, also gives an Avrami coefficient of $n = 1$, confirming the one-dimensional growth of AzD6. This result characterizes the transfer of the nucleation and growth types of SWS depending on I_{UV}, but it is still not clear why the Avrami coefficient varies so discretely with I_{UV}. This important fundamental question is left open.

IV. CONCLUSIONS

We clarified the light-induced dynamic extinction and growth or regeneration processes of surface nanostructures

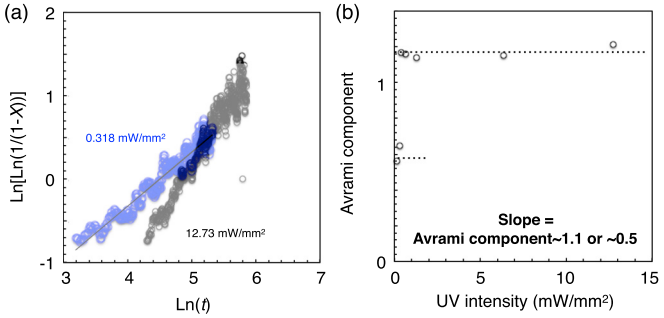

FIG. 7. (a) Avrami analysis of SH signals upon relaxing from the signal level at time 0 to the initial level [saturated level in Fig. 6(a)]. This tracks the regeneration and growth processes of the AzD6 SWS. The linear fitting (lines) gives Avrami coefficient $n \sim 1.1$ or 0.5. (b) Avrami coefficients as a function of UV intensity.

composed of polarly layered AzD6 molecules. Our experimental and analytical results from complementary methods lead to three important conclusions. First, there are wetting sheets of a surface-specific lamellar structure of AzD6. The wetting sheets are inherently polar. Second, the extinction and growth or regeneration processes of the wetting sheets can be tuned by light and are reversible. This results in the polar-nonpolar switching of the surface. Third, by controlling the light intensity, the volume of the wetting sheets on surfaces can be controlled. As a result, the polar orientation of host anisotropic molecules can be controlled by the surface-localized nanostructures. Our results offer fundamental insights into the dynamics of surface nanostructures, which may help to understand many surface-related phenomena, such as those in organic photovoltaics based on mesogenic semiconductors [34–36], and provide a method to control the transient surface wetting structures with light.

ACKNOWLEDGMENTS

We sincerely thank Professor H. Takezoe of the Toyota Physical and Chemical Research Institute and Professor A. Eremin of Otto von Guericke University Magdeburg for valuable discussions. The synchrotron radiation experiments were performed at the BL45XU beamline of SPring-8 with the approval of RIKEN (Proposal No. 20150086). This work was supported by JSPS KAKENHI Grant No. 16H06037.

[1] K. Ichimura, Chem. Rev. **100**, 1847 (2000).
[2] W. J. Gibbons, P. J. Shannon, S.-T. Sun, and B. J. Swetlin, Nature (London) **351**, 49 (1991).
[3] C. Culbreath, N. Glazar, and H. Yokoyama, Rev. Sci. Instrum. **82**, 126107 (2011).
[4] J. Kobashi, H. Yoshida, and M. Ozaki, Nat. Photon. **10**, 389 (2016).
[5] S. Palagi, A. G. Mark, S. Y. Reigh, K. Melde, T. Qiu, H. Zeng, C. Parmeggiani, D. Martella, A. Sanchez-Castillo, N. Kapernaum, F. Giesselmann, D. S. Wiersma, E. Lauga, and P. Fischer, Nat. Mater. **15**, 647 (2016).
[6] S. Samitsu, Y. Takanishi, and J. Yamamoto, Nat. Mater. **9**, 816 (2010).
[7] A. Eremin, P. Hirankittiwong, N. Chattham, H. Nádasi, R. Stannarius, J. Limtrakul, O. Haba, K. Yonetake, and H. Takezoe, Proc. Natl. Acad. Sci. **112**, 1716 (2015).
[8] F. Weigert, Verh. Dtsch. Phys. Ges. **21**, 479 (1919).
[9] A. Shishido, Polymer J. **42**, 525 (2010).
[10] T. G. Pedersen, P. M. Johansen, N. C. R. Holme, P. S. Ramanujam, and S. Hvilsted, Phys. Rev. Lett. **80**, 89 (1998).
[11] K. G. Yager and C. J. Barret, Curr. Opinion Sol. St. Mat. Sci. **5**, 487 (2001).
[12] J. Kumar, L. Li, X. Jiang, D. Kim, T. Lee, and S. Tripathy, Appl. Phys. Lett. **72**, 2096 (1998).
[13] Y. Momoi, M. Kwak, D. Choi, Y. Choi, K. Jeong, T. Koda, O. Haba, and K. Yonetake, J. Soc. Inf. Disp. **20**, 486 (2012).
[14] W. Li, S. Nagano, K. Yonetake, and T. Seki, Mol. Cryst. Liq. Cryst. **563**, 112 (2012).
[15] G. Lee, F. Araoka, K. Ishikawa, Y. Momoi, O. Haba, K. Yonetake, and H. Takezoe, Part. Part. Syst. Charact. **30**, 847 (2013).
[16] J. Noh, V. S. R. Jampani, O. Haba, K. Yonetake, H. Takezoe, and J. P. F. Lagerwall, J. Mol. Liq. **267**, 197 (2018).
[17] S. Aya, Y. Sasaki, H. Takezoe, K. Ishikawa, K. Ema, T. Hikima, M. Takata, and F. Araoka, Langmuir **32**, 10545 (2016).
[18] K. Kočevar, R. Blinc, and I. Muševič, Phys. Rev. E **62**, R3055 (2000).
[19] S. M. Hues, R. J. Colton, E. Meyer, and H.-J. Güntherodt, MRS Bull. **18**, 41 (1993).
[20] H. L. Ong, A. J. Hurd, and R. B. Meyer, J. Appl. Phys. **57**, 186 (1985).
[21] T. Fujisawa, K. Inoue, T. Oka, H. Iwamoto, T. Uruga, T. Kumasaka, Y. Inoko, N. Yagi, M. Yamamoto, and T. Ueki, J. Appl. Crystallogr. **33**, 797 (2000).
[22] See Supplemental Material at http://link.aps.org/supplemental/10.1103/PhysRevE.98.052701 for a movie of the H state induced simultaneously.
[23] K. Yonetake, T. Masuko, T. Morishita, K. Suzuki, M. Ueda, and R. Nagahata, Macromolecules **32**, 6578 (1999).
[24] W. Li, T. Dohi, M. Hara, S. Nagano, O. Haba, K. Yonetake, and T. Seki, Macromolecules **45**, 6618 (2012).
[25] A. Yamaguchi, N. Uehara, J. Yamamoto, and A. Yoshizawa, Chem. Mater. **19**, 6445 (2007).
[26] H. Nadasi, R. Stannarius, A. Eremin, A. Ito, K. Ishikawa, O. Haba, K. Yonetake, H. Takezoe, and F. Araoka, Phys. Chem. Chem. Phys. **19**, 7597 (2017).
[27] S. Saito, S. Nobusue, E. Tsuzaka, C. Yuan, C. Mori, M. Hara, T. Seki, C. Camacho, S. Irle, and S. Yamaguchi, Nat. Commun. **7**, 12094 (2016).
[28] P. Atkins and J. de Paula, *Physical Chemistry, Volume 1: Thermodynamics and Kinetics* (W. H. Freeman, New York, 2011).
[29] M. Avrami, J. Chem. Phys. **7**, 1103 (1939).
[30] M. Avrami, J. Chem. Phys. **8**, 212 (1940).
[31] M. Avrami, J. Chem. Phys. **9**, 177 (1941).
[32] A. N. Kolmogorov, Izv. Akad. Nauk SSSR, Ser. Mat. **3**, 355 (1937).
[33] J. Torrens-Serra, S. Venkataraman, M. Stoica, U. Kuehn, S. Roth, and J. Eckert, Materials **4**, 2231 (2011).
[34] V. Vohra, K. Kawashima, T. Kakara, T. Koganezawa, I. Osaka, K. Takimiya, and H. Murata, Nat. Photon. **9**, 403 (2015).
[35] F. Wang, K. Hashimoto, H. Segawa, and K. Tajima, ACS Appl. Mater. Interfaces **10**, 8901 (2018).
[36] S. Izawa, K. Nakano, K. Suzuki, Y. J. Chen, T. Kikitsu, D. Hashizume, T. Koganezawa, T.-Q. Nguyen, and K. Tajima, Sci. Rep. **8**, 481 (2018).